core. The shear stress variations in the core are plotted in Fig. 7 for $h/h_f = 10$. The interface shear stress reduces as the E_h/E_0 ratio is increased. The maximum reduction of 20% occurs for the case $E_h/E_f = 1$, for which the core elastic modulus varies exponentially from $E_0 = E_f/1000$ at the center to $E_h = E_f$ at the core–face-sheet interface. Figure 8 shows the ratio of shear stress at the interface for different values of E_h/E_0 ratio and h/h_f ratio. The reduction in shear stress at the interface increases with increase in h/h_f ratio (or for beams when the face sheet is significantly thinner than the core). For the example problem the reduction in interface shear stress is 42 and 63% for h/h_f values of 20 and 40, respectively.

Summary

The elasticity solution obtained for a simple functionally graded beam has been extended for a sandwich configuration. The stresses calculated from the elasticity solution were used to demonstrate the reduction in face-sheet–core interface shear stress possible by functionally grading the sandwich core elastic properties.

Acknowledgments

This research was supported by NASA Langley Research Center Grant NAG-1-1887 to the University of Florida. The authors are thankful to D. R. Ambur, Head, Mechanics and Durability Branch, for his input and encouragement.

Reference

[1]Sankar, B. V., "An Elasticity Solution for Functionally Graded Beams," *Composites Science and Technology*, Vol. 61, No. 5, 2001, pp. 689–696.

K. N. Shivakumar
Associate Editor

Triangular Shell Element for Large Rotations Analysis

R. Levy*
Technion—Israel Institute of Technology, 32000 Haifa, Israel
and
E. Gal†
Ben Gurion University of the Negev, 84105 Beer Sheva, Israel

I. Introduction

GEOMETRICALLY nonlinear analysis of shells for small strains and large rotations can be described in terms of three key steps: derivation of the geometric stiffness matrix, iterative solution of the governing equations, and stress retrieval and updating. It is the derivation of the geometric stiffness matrix and stress retrieval for thin shells that is the focus of this Note. Here the geometry of the shell surface is approximated with flat triangular shell elements, each of which is composed of a membrane and a plate element.

In the literature a number of methods exist for the derivation of the geometric stiffness matrix of shells. These are based on classical nonlinear shell theory represented as a two-dimensional Cosserat surface, three-dimensional elasticity degenerate shells, and perturbation methods. The excellent comprehensive review by Ibrahimbegović[1] addresses the various approaches and the related complex issues involved.

The present approach is based on gradient methods that are equivalent to perturbation methods (e.g., Green et al.[2]), where first-order perturbation analysis corresponds to first-order Taylor-series linearization. Related to the present approach is the corotational realm (for example, see Bathe and Ho[3] and Peng and Crisfield[4]).

The geometric stiffness matrix is derived by first performing a load perturbation on the linear equilibrium shell equations with respect to the local coordinates system to yield the in-plane geometric stiffness matrix. Then out-of-plane considerations that involve the effect of rigid-body rotations on member forces complete the local geometric stiffness matrix formulation. As for stress retrieval, the linear equations of elasticity are used throughout because of the a priori removal of rigid-body rotations by a special procedure, which is developed later. These two features make this approach unique compared to other methods of similar general characteristics. Finally a computer program featuring incremental analysis and Newton's method, geometric effects, pure deformations isolation, internal stresses retrieval, and updating of nodal forces and coordinates was coded to implement the derivations described herein and used to solve a number of problems that appeared in the literature with practically matching results.

II. Geometric Stiffness Matrix of the Flat Triangular Shell Element

Load perturbation of the shell equilibrium equations leads to the well-established definition of the geometric stiffness matrix as the gradient with respect to the global coordinates of the nodal force vector when stresses are held fixed.[5] To circumvent the taking of impossible derivatives of the three-dimensional rotation matrix, the load perturbation method is applied with respect to local coordinates. In that case an additional out-of-plane effect has to be considered. This out-of-plane effect is physically the change in the nodal force vector as a result of the rigid-body rotation. The geometric stiffness matrix is thus composed of four individual matrices, two in-plane (IP) and two out-of-plane (OP) matrices for the membrane and plate elements, respectively:

$$\left[\boldsymbol{K}_G^e\right]_{\text{TOTAL}}^{\text{shell}} = \left[\boldsymbol{K}_G^e\right]_{\text{IP}}^{\text{mem}} + \left[\boldsymbol{K}_G^e\right]_{\text{IP}}^{\text{plate}} + \left[\boldsymbol{K}_G^e\right]_{\text{OP}}^{\text{mem}} + \left[\boldsymbol{K}_G^e\right]_{\text{OP}}^{\text{plate}} \tag{1}$$

A. In-Plane Contribution of the Flat Triangular Membrane Element

The nodal force vector of the simple plane stress triangular finite element (CST) that is described by Zienkiewicz[6] is used as the membrane element is given as

$$\boldsymbol{F}^e = \frac{t}{2}\begin{Bmatrix} b_i\sigma_x + c_i\tau_{xy} \\ c_i\sigma_y + b_i\tau_{xy} \\ \vdots \\ b_j\sigma_x + c_j\tau_{xy} \\ c_j\sigma_y + b_j\tau_{xy} \\ \vdots \\ b_m\sigma_x + c_m\tau_{xy} \\ c_m\sigma_y + b_m\tau_{xy} \end{Bmatrix} \begin{matrix} \\ \text{row } i \\ \\ \\ \text{row } j \\ \\ \\ \text{row } m \end{matrix} \tag{2}$$

where the coefficients b_r, c_r $r = i, j, m$ are explicitly defined in Ref. 6; t is the thickness of the element; and σ_x, σ_y, τ are its stresses. The gradient of Eq. (2) that is taken in a rather straightforward manner[6] to yield a 6×6 in-plane contribution to the geometric stiffness matrix of the membrane is

$$\left[\boldsymbol{K}_G^e\right]_{\text{IP}}^{\text{mem}} = \nabla \boldsymbol{F}_{\text{mem}}^e = \begin{bmatrix} \boldsymbol{0} & \boldsymbol{A}_{\text{IP}}^{\text{mem}} & -\boldsymbol{A}_{\text{IP}}^{\text{mem}} \\ -\boldsymbol{A}_{\text{IP}}^{\text{mem}} & \boldsymbol{0} & \boldsymbol{A}_{\text{IP}}^{\text{mem}} \\ \boldsymbol{A}_{\text{IP}}^{\text{mem}} & -\boldsymbol{A}_{\text{IP}}^{\text{mem}} & \boldsymbol{0} \end{bmatrix}$$

$$\boldsymbol{A}_{\text{IP}}^{\text{mem}} = \frac{t}{2}\begin{bmatrix} -\tau & \sigma_x \\ -\sigma_y & \tau \end{bmatrix} \tag{3}$$

Received 19 June 2002; revision received 7 July 2003; accepted for publication 24 July 2003.

*Associate Professor, Faculty of Civil and Environmental Engineering; cvrlevy@tx.technion.ac.il. Member AIAA.

†Postdoctoral Fellow, Department of Structural Engineering, Faculty of Engineering.

B. In-Plane Contribution of the Flat Triangular Plate Bending Element

The discrete Kirchhoff theory (DKT) triangular plate element that is described by Batoz et al.[7] is chosen to fulfill the flexural needs of the shell. The load perturbation of the element force vector for fixed stresses is given in integral form as

$$\begin{aligned} \mathrm{d}\boldsymbol{F}^e_{\text{plate}} &= \nabla \boldsymbol{F}^e_{\text{plate}} \cdot \mathrm{d}\boldsymbol{x} = [\boldsymbol{K}_G]^{\text{plate}}_{\text{IP}} \cdot \mathrm{d}\boldsymbol{x} \\ &= \sum_{r=i,j,m} \left[\frac{\partial}{\partial x_r} \left(2A \int_0^1 \int_0^{1-\eta} \boldsymbol{B}^T_{\text{plate}} \boldsymbol{M}_{\text{fixed}} \, \mathrm{d}\xi \, \mathrm{d}\eta \right) \mathrm{d}x_r \right. \\ &\quad \left. + \frac{\partial}{\partial y_r} \left(2A \int_0^1 \int_0^{1-\eta} \boldsymbol{B}^T_{p} \boldsymbol{M}_{\text{fixed}} \, \mathrm{d}\xi \, \mathrm{d}\eta \right) \mathrm{d}y_r \right] \end{aligned} \tag{4}$$

where ξ and η are the usual area coordinates; $\boldsymbol{B}_{\text{plate}}$ appears explicitly in Ref. 7; $\boldsymbol{M} = (t^3/12)\boldsymbol{D}\boldsymbol{B}_{\text{plate}}\boldsymbol{q}^e = \{M_{xx}, M_{yy}, M_{xy}\}^T$; and $\boldsymbol{q}_e = \{w_1 \ \theta_{x1} \ \theta_{y1} \ w_2 \ \theta_{x2} \ \theta_{y2} \ w_3 \ \theta_{x3} \ \theta_{y3}\}$. The expressions for the individual terms of the gradient were obtained in closed form using symbolic algebra.

C. Out-of-Plane Contribution of the Flat Triangular Membrane Element

The out-of-plane contribution can be computed using the relationship from rigid-body mechanics,[8] which states that the change in a vector $\boldsymbol{G}$ caused by a small rotation is given by

$$\mathrm{d}\boldsymbol{G} = \boldsymbol{\omega} \times \boldsymbol{G} \tag{5}$$

where $\boldsymbol{\omega}$ is the rigid-body rotation vector caused by changes in the geometry. Using a small rotations vector is in harmony with perturbation theory and the first-order (gradient) definition of the geometric stiffness matrix because the small rotations vector is a one-term Taylor expansion of Euler's finite rotations pseudovector. The components of the rigid-body rotations can be obtained in terms of the joint displacements as

$$\begin{aligned} \omega_x &= [(c-e)/ea]\delta_{iz} - (c/ea)\delta_{jz} + (1/a)\delta_{mz} \\ \omega_y &= (a/ea)\delta_{iz} - (a/ea)\delta_{jz}, \qquad \omega_z = \theta_{iz} \end{aligned} \tag{6}$$

where $\delta_{ji} = \delta_{jz} - \delta_{iz}$; $\delta_{mi} = \delta_{mz} - \delta_{iz}$; and δ_{rz} is the displacement in the z direction of node r. The third component is chosen arbitrarily as the local z rotation of node i. For the membrane this component is included in Eq. (3) and is therefore taken as zero.

For each node the forces can be written as $\boldsymbol{F}^{\text{mem}}_r = F_{rx}\boldsymbol{i} + F_{ry}\boldsymbol{j}$ and the rotations for the whole element as $\boldsymbol{\omega}^{\text{mem}}_r = \omega_x \boldsymbol{i} + \omega_y \boldsymbol{j}$. Applying Eq. (5) yields the out-of-plane stiffness contribution of the membrane:

$$\begin{aligned} \mathrm{d}\boldsymbol{F}^e &= [\boldsymbol{K}_G]^{\text{mem}}_{\text{OP}} \cdot \boldsymbol{\delta}^e = \begin{bmatrix} \boldsymbol{F}^{e\,\text{mem}}_i \\ \boldsymbol{F}^{e\,\text{mem}}_j \\ \boldsymbol{F}^{e\,\text{mem}}_m \end{bmatrix} \boldsymbol{\omega} = \boldsymbol{A}^{\text{mem}} \boldsymbol{\delta}^e \\ &= \begin{bmatrix} \boldsymbol{A}^{\text{mem}}_i & \boldsymbol{A}^{\text{mem}}_j & \boldsymbol{A}^{\text{mem}}_m \end{bmatrix} \boldsymbol{\delta}^e \end{aligned} \tag{7}$$

where $\boldsymbol{F}^{e\,\text{mem}}_r$ is a 6×3 matrix with zero entries in the last three rows and the cross product $-\boldsymbol{F}^{\text{mem}}_r \times \boldsymbol{\omega}$ in the first three rows.

D. Out-of-Plane Contribution of the Plate Element

The same procedure is used here as in the preceding section. For each node the forces can be written as $\boldsymbol{F}^{\text{plate}}_r = F_{rz}\boldsymbol{k}$ and the moments as $\boldsymbol{M}^{\text{plate}}_r = M_{rx}\boldsymbol{i} + M_{ry}\boldsymbol{j} + M_{rz}\boldsymbol{k}$ and rotations for the whole element as $\boldsymbol{\omega}^{\text{plate}}_r = \omega_x \boldsymbol{i} + \omega_y \boldsymbol{j} + \omega_z \boldsymbol{k}$. Applying Eq. (5) yields the out-of-plane stiffness contribution $[\boldsymbol{K}_G]^{\text{plate}}_{\text{OP}}$ of the plate that has the same form as Eq. (7). Here $\boldsymbol{F}^{e\,\text{plate}}_r$ is a 6×3 matrix with the cross product $-\boldsymbol{F}^{\text{plate}}_r \times \boldsymbol{\omega}$ in the first three rows and the cross product $-\boldsymbol{M}^{\text{plate}}_r \times \boldsymbol{\omega}$ in the last three rows.

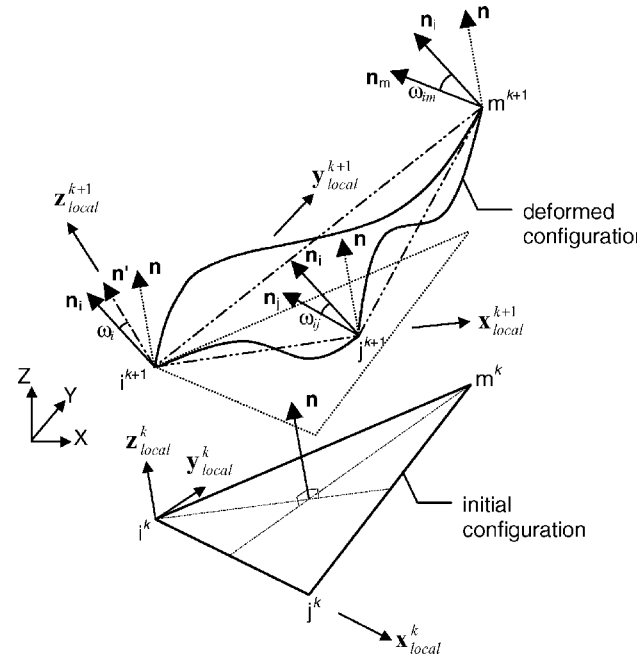

Fig. 1 Pure flexural rotations of the shell element.

III. Removal of Rigid-Body Rotations

If the concept of small strains and large rotations (in an incremental manner of course) is to be pursued literally, the stress retrieval should follow from linear constitutive relations, i.e., $\boldsymbol{\sigma} = \boldsymbol{D}\boldsymbol{\varepsilon}$, for the membrane, where $\boldsymbol{\sigma}$ comprises the stress components σ_x, σ_y, and τ and $\boldsymbol{\varepsilon}$ comprises the strain components ε_x, ε_y, and γ_{xy}, respectively, and $M = (t^3/12)\boldsymbol{D}\boldsymbol{B}_{\text{plate}}\,\boldsymbol{q}_e$ for the plate, where $\boldsymbol{q}_e$ is the pure local deformation vector free of rigid-body rotations and includes one lateral displacement and two in-plane rotations at each node. Obtaining $\boldsymbol{q}_e$ constitutes a novel contribution and will be presented in some detail.

Figure 1 describes two positions of a given element at two consecutive iterations k and $k+1$ with normal unit vectors $\boldsymbol{n}$ and $\boldsymbol{n}'$, respectively. The rigid-body motion of the element is not fully determined by the unit vector $\boldsymbol{n}'$ because rotation about the element plane is still possible given $\boldsymbol{n}'$. Let the small deformational rotation vector $\boldsymbol{\omega}_i$, which is actually the pure rotation at node i in global coordinates, describe the rotation between the vector $\boldsymbol{n}'$ and $\boldsymbol{n}_i$ with the properties

$$\boldsymbol{\omega}_i = \arcsin(\|\boldsymbol{n}_i \times \boldsymbol{n}'\|) \cdot \frac{\boldsymbol{n}_i \times \boldsymbol{n}'}{\|\boldsymbol{n}_i \times \boldsymbol{n}'\|} \tag{8}$$

The pure rotations at the other elemental nodes j and m can be computed relative to node i as

$$\boldsymbol{\omega}_r = \boldsymbol{\omega}_i + \boldsymbol{\omega}_{ri}, \qquad r = j, m \tag{9}$$

Here $\boldsymbol{\omega}_{ri}$ describes the relative rotation of joint r with respect to joint i and is the pseudovector form (Euler's theorem; see Ref. 9) of the compound rotations $\boldsymbol{R}^T_j \boldsymbol{R}_i$. Let this now available compound rotations matrix be called $\boldsymbol{R}_{ij}$ so that $\boldsymbol{R}_{ij} = \boldsymbol{R}^T_j \boldsymbol{R}_i$. Then the unit vector describing the rigid-body rotation is given as[5]

$$\boldsymbol{n}^*_{ji} = \bar{\boldsymbol{\omega}}_{ji} / \|\bar{\boldsymbol{\omega}}_{ji}\| \tag{10}$$

where

$$\bar{\boldsymbol{\omega}}_{ji} = \left(R^T_{ij,23} - R^T_{ij,32}\right)\boldsymbol{i} + \left(R^T_{ij,31} - R^T_{ij,13}\right)\boldsymbol{j} + \left(R^T_{ij,21} - R^T_{ij,12}\right)\boldsymbol{k} \tag{11}$$

and the magnitude of rotation as

$$\alpha_{ji} = \cos^{-1}\left[\left(R^T_{ij,11} + R^T_{ij,22} + R^T_{ij,33} - 1\right)/2\right] \tag{12}$$

Finally, the relative rotation vector becomes

$$\omega_{ji} = n^{*}_{ji}\alpha_{ji} \tag{13}$$

The pure rotations vector is finally transformed into the present local coordinate system.

IV. Examples

Five examples are included in this section. They were solved using the computer program (SHELLNL) that was coded, and they were chosen because of their diversity: analytical, experimental, and computational.

A. Spherical Shell

Leicester[10] used Fourier transforms to solve the nonlinear differential equations of a spherical cap having a square base whose side is 61.8034 in., which originates from a sphere of radius $R = 100$ in. It is subjected to a concentrated load at the crown with all edges hinged and immovable. This example was run using a 10×10 grid on a quarter of the cap with the following physical and geometrical constants: Young's modulus $E = 10^3$ ksi, Poisson's ratio $\nu = 0.3$, and a thickness of 3.9154 in. Figure 2 shows how well results compare.

B. Shallow Spherical Shell: An Analytical Case

Mescall[11] reported analytic results for large displacement analysis of a spherical shallow shell subjected to a concentrated load at the crown. Two cases of support conditions were considered: rigid supports and vertically restrained supports. The geometry of the shallow shell is drawn as the intersection of a cone whose tip lies at the center of a shell of radius 4.76 in. and having a tip angle of 21.8 deg. The thickness of the shell is taken as $t = 0.01576$ in., Young's modulus $E = 10^7$ psi, and Poisson's ratio $\nu = 0.3$. Figure 3 shows a comparison for the rigidly supported shell that strain hardens and the vertically restrained shell that snaps.

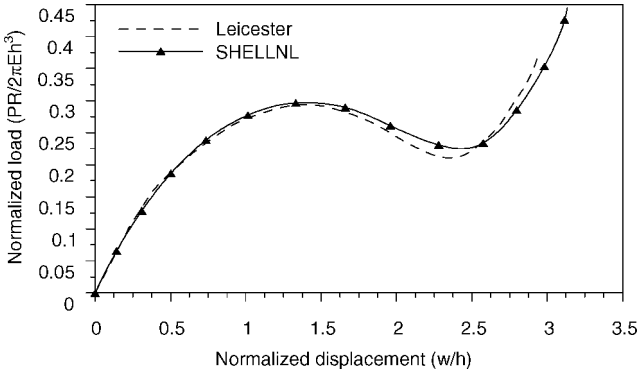

Fig. 2 Displacement at crown of spherical shell.

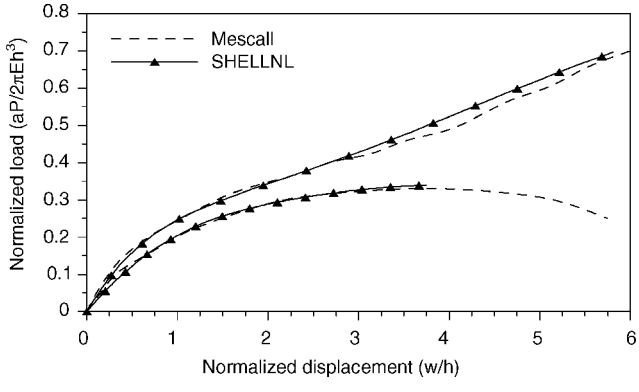

Fig. 3 Displacements of Mescall's shell.

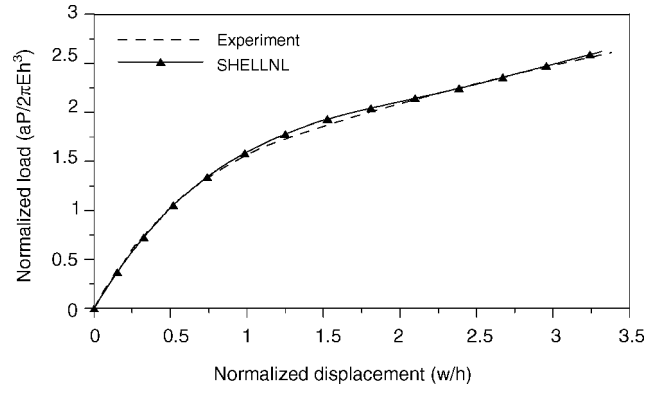

Fig. 4 Displacements of Penning's experiment.

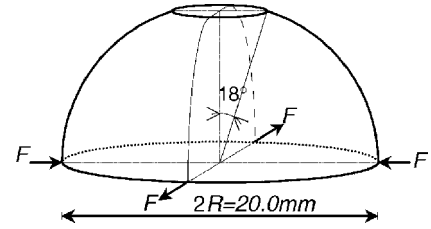

Fig. 5 Open hemispherical shell.

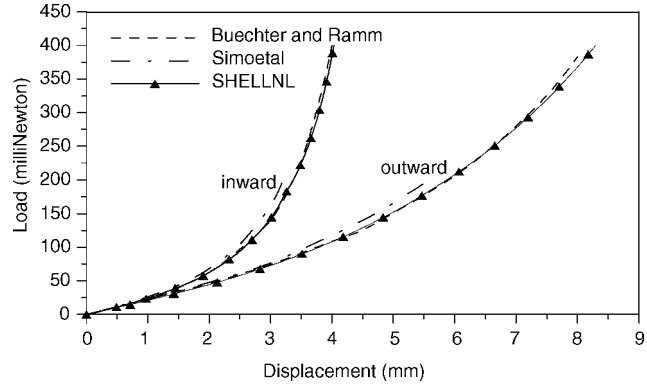

Fig. 6 Open hemispherical shell.

C. Shallow Spherical Shell: An Experimental Case

Penning[12] performed an experiment on a shallow spherical shell with a circular base of 4.0 in. that is cut from a sphere of radius 19.8 in. The thickness of the shell is taken as $t = 0.01576$ in, Young's modulus $E = 10^7$ psi, and Poisson's ratio $\nu = 0.3$. Results are displayed in Fig. 4.

D. Open Hemispherical Shell

A hemispherical shell (Fig. 5) with an 18-deg opening at the top is loaded by two orthogonal pairs of diametrically opposite equal forces. One pair is directed inwards, whereas the other pair is directed outward. Using symmetry, only one-quarter of the shell was loaded and modeled using 16 latitudes by 16 longitudes. In this case $E = 6.825 \times 10^6$ mN/mm^2; $t = 0.04$ mm; and Poisson's ratio of 0.3. Results are compared in Fig. 6 with those of Buechter and Ramm[13] and Simo[14] et al.

V. Conclusions

This Note showed that gradient methods can be used to form the geometric stiffness matrix without recourse to methods of nonlinear elasticity provided that small strains are incurred and that linear relations for stress retrieval can be used because the isolation of pure deformations, free of rigid-body rotations, is ensured using the technique presented.

The in-plane geometric stiffness matrix is a first-order linearization of the perturbed nodal force vector in local coordinates; the out-of-plane stiffness matrix is a first-order correction stemming from the change in the nodal force vector caused by small rigid-body rotations. This approach is thus first-order complete especially because Newton's method is used for analysis. Although this approach depends on an a priori chosen linear elastic finite element, it is independent of large strain formulations.

References

[1]Ibrahimbegović, A., "Stress Resultant Geometrically Exact Shell Theory for Finite Rotations and Its Finite Element Implementation," *Applied Mechanics Reviews*, Vol. 50, No. 4, 1997, pp. 199–226.

[2]Green, A. E., Knops, R. J., and Laws, N., "Large Deformations, Superimposed Small Deformations, and Stability of Elastic Rods," *International Journal of Solids and Structures*, Vol. 4, 1968, pp. 555–557.

[3]Bathe, K. J., and Ho, L. W., "A Simple and Effective Element for Analysis of General Shell Structures," *Computers and Structures*, Vol. 13, 1980, pp. 673–681.

[4]Peng, X., and Crisfield, M. A., "A Consistent Co-Rotational Formulation for Shell Using the Constant Stress/Constant Moment Triangle," *International Journal of Numerical Metheds in Engineering*, Vol. 35, 1992, pp. 1829–1847.

[5]Levy, R., and Spillers, W. R., *Analysis of Geometrically Nonlinear Structures*, Chapman and Hall, New York, 1994.

[6]Zienkiewicz, O. C., *The Finite Element Method*, 3rd ed., McGraw–Hill, New Nork, 1977.

[7]Batoz, J. L., Bathe, K. J., and Ho, L. W., "A Study of Three Noded Triangular Plate Bending Elements," *International Journal of Numerical Methods in Engineering*, Vol. 15, 1980, pp. 1771–1812.

[8]Goldstein, H., *Classical Mechanics*, Addison Wesley Longman, Reading, MA, 1950.

[9]Noble, B., *Applied Linear Algebra*, Prentice–Hall, Upper Saddle River, NJ, 1969, p. 421.

[10]Leicester, R. H., "Finite Deformations of Shallow Shells," *Proceedings of the ASCE*, Vol. 94 (EM6), 1968, pp. 1409–1423.

[11]Mescall, J. F., "Large Deflections of Spherical Shells Under Concentrated Loads," *Journal of Applied Mechanics*, Vol. 32, 1965, pp. 936–938.

[12]Penning, F. A., "Experimental Buckling Modes of Clamped Shallow Shells Under Concentrated Load," *Journal of Applied Mechanics*, Vol. 33, 1966, pp. 247–304.

[13]Buechter, N., and Ramm, E., "Shell Theory versus Degeneration—A Comparison in Large Rotation Finite Element Analysis," *International Journal for Numerical Methods in Engineering*, Vol. 34, 1992, pp. 39–59.

[14]Simo, J. C., Fox, D. D., and Rifai, M. S., "On a Stress Resultant Geometrically Exact Shell Model. Part III: Computational Aspects of the Nonlinear Theory," *Computer Methods in Applied Mechanics and Engineering*, Vol. 79, 1990, pp. 21–70.

S. Saigal
Associate Editor

Errata

Effect of Surface Roughness on Unseparated Shock-Wave/Turbulent Boundary-Layer Interactions

H. Babinsky
University of Cambridge, Cambridge, England CB2 1PZ, United Kingdom
and
G. R. Inger
Iowa State University, Ames, Iowa 50011-3231

[AIAA Journal, 40(8), pp. 1567–1573 (2002)]

THE authors would like to thank Angela D. McConnell for providing all of the original data as part of her M.Phil. research at Cambridge University (Thesis title: "Roughness Effects on Impinging Shock Wave/Turbulent Boundary Layer Interactions"). Further details can be found in Ref. 6 of our original paper:

Babinsky, H., Inger, G. R., and McConnell, A. D., "A Basic Experimental/Theoretical Study of Rough Wall Turbulent Shock/Boundary Layer Interaction," *Proceedings of the 22nd International Symposium on Shock Waves*, London, 1999, pp. 885–889.

The authors apologize for failing to appropriately acknowledge Miss McConnell's contribution in the original paper.